REPORT

Bi-allelic variants in the ER quality-control mannosidase gene *EDEM3* cause a congenital disorder of glycosylation

Daniel L. Polla,[1,2,22] Andrew C. Edmondson,[3,22] Sandrine Duvet,[4] Michael E. March,[5] Ana Berta Sousa,[6,7] Anna Lehman,[8] CAUSES Study, Dmitriy Niyazov,[9] Fleur van Dijk,[10] Serwet Demirdas,[11] Marjon A. van Slegtenhorst,[11] Anneke J.A. Kievit,[11] Celine Schulz,[4] Linlea Armstrong,[8] Xin Bi,[12] Daniel J. Rader,[5,12,13] Kosuke Izumi,[3] Elaine H. Zackai,[3] Elisa de Franco,[14] Paula Jorge,[15,16] Sophie C. Huffels,[1] Marina Hommersom,[1] Sian Ellard,[14,17] Dirk J. Lefeber,[18,19] Avni Santani,[20,21] Nicholas J. Hand,[13,22] Hans van Bokhoven,[1,22] Miao He,[21,22,*] and Arjan P.M. de Brouwer[1,22,*]

Summary

EDEM3 encodes a protein that converts $Man_8GlcNAc_2$ isomer B to $Man_{7-5}GlcNAc_2$. It is involved in the endoplasmic reticulum-associated degradation pathway, responsible for the recognition of misfolded proteins that will be targeted and translocated to the cytosol and degraded by the proteasome. In this study, through a combination of exome sequencing and gene matching, we have identified seven independent families with 11 individuals with bi-allelic protein-truncating variants and one individual with a compound heterozygous missense variant in *EDEM3*. The affected individuals present with an inherited congenital disorder of glycosylation (CDG) consisting of neurodevelopmental delay and variable facial dysmorphisms. Experiments in human fibroblast cell lines, human plasma, and mouse plasma and brain tissue demonstrated decreased trimming of $Man_8GlcNAc_2$ isomer B to $Man_7GlcNAc_2$, consistent with loss of EDEM3 enzymatic activity. In human cells, $Man_5GlcNAc_2$ to $Man_4GlcNAc_2$ conversion is also diminished with an increase of $Glc_1Man_5GlcNAc_2$. Furthermore, analysis of the unfolded protein response showed a reduced increase in *EIF2AK3* (*PERK*) expression upon stimulation with tunicamycin as compared to controls, suggesting an impaired unfolded protein response. The aberrant plasma N-glycan profile provides a quick, clinically available test for validating variants of uncertain significance that may be identified by molecular genetic testing. We propose to call this deficiency EDEM3-CDG.

The endoplasmic reticulum-associated degradation (ERAD) pathway recognizes misfolded proteins that will be targeted and translocated to the cytosol and degraded by the proteasome.[1–4] The best characterized system is dedicated to N-linked glycoproteins: the glycoprotein ERAD (gpERAD) pathway. Proteins that fail to fold or assemble properly are subjected to degradation via specific trimming of high-mannose-type glycans in the lumen of the ER.[5,6] In mammals, EDEM2 and ERmanI are known to primarily catalyze the first step, conversion of $Man_9GlcNAc_2$ (M9) to $Man_8GlcNAc_2$ isomer B (M8B).[7–9] EDEM3 and EDEM1 are further involved in catalyzing the second step, the conversion of M8B to $Man_7GlcNAc_2$ (M7).[7–12] These products are then recognized by lectin OS-9 in the ER lumen and targeted for degradation in the cytosol.[13]

Cells can degrade misfolded proteins from the secretory pathway by using the glycan-dependent and glycan-independent ERAD pathways.[14–16] The presence of misfolded ER proteins is harmful to cells and is involved in several congenital disorders of glycosylation (CDGs),[17–20] such as PMM2-CDG (MIM: 212065), MPI-CDG (MIM: 602579), ALG6-CDG (MIM: 603147), DPM1-CDG (MIM: 608799),

[1]Department of Human Genetics, Donders Institute for Brain, Cognition, and Behavior, Radboud University Medical Center, 6500 HB Nijmegen, the Netherlands; [2]CAPES Foundation, Ministry of Education of Brazil, Brasília, Brazil; [3]Department of Pediatrics, Division of Human Genetics, Children's Hospital of Philadelphia, Philadelphia, PA 19104, USA; [4]Université de Lille, CNRS, UMR 8576 – UGSF – Unité de Glycobiologie Structurale et Fonctionnelle, F-59000 Lille, France; [5]Center for Applied Genomics, Children's Hospital of Philadelphia, Philadelphia, PA 19104, USA; [6]Serviço de Genética Médica, Hospital de Santa Maria, Centro Hospitalar Universitário Lisboa Norte, 649-035 Lisboa, Portugal; [7]Faculdade de Medicina da Universidade de Lisboa, 1649-028 Lisboa, Portugal; [8]Department of Medical Genetics, University of British Columbia, Vancouver, BC V6H 3N1, Canada; [9]Tulane School of Medicine, University of Queensland, 1315 Jefferson Highway, New Orleans, LA 70121, USA; [10]North West Thames Regional Genetics Service, London North West University Healthcare NHS Trust, Watford Road, Harrow, HA1 3UJ London, UK; [11]Department of Clinical Genetics, Erasmus University Medical Center, 3015 Rotterdam, the Netherlands; [12]Department of Medicine, Perelman School of Medicine, University of Pennsylvania, Philadelphia, PA 19104, USA; [13]Department of Genetics, Perelman School of Medicine, University of Pennsylvania, Philadelphia, PA 19104, USA; [14]Department of Molecular Genetics, Royal Devon and Exeter NHS Foundation Trust, Barrack Road, EX2 5DW Exeter, UK; [15]Centro de Genética Médica Jacinto de Magalhães, Centro Hospitalar do Porto, CHP, E.P.E., 4099-028 Porto, Portugal; [16]Unit for Multidisciplinary Research in Biomedicine, Abel Salazar Institute of Biomedical Sciences, University of Porto, 4099-028 Porto, Portugal; [17]College of Medicine and Health, University of Exeter, Barrack Road, EX2 5DW Exeter, UK; [18]Department of Neurology, Donders Institute for Brain, Cognition, and Behavior, Radboud University Medical Center, 6525 GA Nijmegen, the Netherlands; [19]Department of Laboratory Medicine, Translational Metabolic Laboratory, Radboud University Medical Center, 6525 GA Nijmegen, the Netherlands; [20]Department of Pathology and Laboratory Medicine, Children's Hospital of Philadelphia, Philadelphia, PA 19104, USA; [21]Department of Pathology and Laboratory Medicine, Perelman School of Medicine, University of Pennsylvania, Philadelphia, PA 19104, USA
[22]These authors contributed equally
*Correspondence: hem@email.chop.edu (M.H.), arjan.debrouwer@radboudumc.nl (A.P.M.d.B.)
https://doi.org/10.1016/j.ajhg.2021.05.010.

ALG12-CDG (MIM: 607143), and DPAGT1-CDG (MIM: 608093). If this degradative process fails to effectively remove misfolded and abnormal proteins from the ER, then the unfolded protein response (UPR) is initiated.[17–20] The UPR is critical to maintain cellular homeostasis. In mammals, three classical ER stress markers are known to reflect induction of the UPR: protein kinase RNA-like endoplasmic reticulum kinase (PERK), activating transcription factor 6 (ATF6), and inositol requiring enzyme 1 (IRE1).[21,22] Upon protein overload in the ER, UPR signaling via the PERK, ATF6, and IRE1 pathways is activated to increase ER capacity, inhibit translation, and stimulate the removal of excess and misfolded proteins.[23–26] Persistent activation of UPR can lead to apoptosis.[27–29]

Here, we describe seven independent families with 11 individuals with bi-allelic protein-truncating variants and one additional individual with a compound heterozygous missense variant in *EDEM3* (MIM: 610214) identified by exome sequencing (Figure 1) and collected through GeneMatcher.[30] The parents or legal guardians provided written informed consent. All relevant approvals from the institutional review boards and ethics committees of the participating institutions were obtained. In affected individuals from families 1 and 2, a bi-allelic frameshift deletion, c.1859del (p.Ile620Thrfs*7), was identified in *EDEM3* (GenBank: NM_025191.3; Figure 1). Additionally, two frameshift variants, c.2001dup (p.Ala668Serfs*9) and c.1369del (p.Arg457Glufs*28), were identified in family 3. In family 4, a bi-allelic nonsense variant, c.940A>T (p.Arg314*), was found, resulting from maternal uniparental isodisomy of chromosome 1. In family 5, a canonical splice site donor variant, c.853+1G>T, and a nonsense variant, c.1407T>A (p.Tyr469*), were identified, and in family 6, a bi-allelic frameshift deletion, c.1382_1385del (p.Phe461Serfs*23) was identified. Finally, in family 7, the compound heterozygous changes c.182A>G (p.Asp61Gly) and c.1366G>A (p.Asp456Asn) were identified. Sanger sequencing showed that the affected individuals were either homozygous or compound heterozygous for the identified *EDEM3* variants. The unaffected parents were all heterozygous carriers. The p.Asp61Gly missense variant was found in six heterozygous individuals, out of 218,508 alleles, in gnomAD (rs777353823) and was predicted to be "disease causing" by MutationTaster[31] but "tolerated'" by SIFT.[32] The p.Asp456Asn missense variant was not present in gnomAD and was predicted to be "disease causing" by both MutationTaster and SIFT. Both are present in the so-called "Glyco_Hydro_47 domain," which is essential for the α-mannosidase activity of the protein.

Affected individuals from family 1 and 2 have the identical c.1859del (p.Ile620Thrfs*7) *EDEM3* variant, but there are no records of inter-familial consanguinity in these families. Comparison of the exome data from two affected individuals from family 1 and from one affected individual from family 2 indicated that these three individuals carried a common identical region of homozygosity of 3.16 Mb (chr1: 182,993,025–186,157,274, Hg19) surrounding *EDEM3*. In addition, 96 healthy control individuals in the Romani population in Portugal were screened for the presence of this variant, among whom one heterozygous allele was detected. Because families 1 and 2 are of Portuguese Romani origin, this suggests a possible founder effect.

All affected individuals presented with developmental delay and/or intellectual disability (ID) and speech delay (Table S1). Hypotonia was present in six out of 12 persons. Dysmorphic facial features, such as narrow palpebral fissures (6/12), epicanthal folds (6/12), increased nasal height (8/12), bulbous nasal tip (6/12), hypoplastic alae nasi (9/12), short philtrum (6/12), thin upper lip (9/12), and retrognathia (6/12) were also found in half or more of the affected individuals. Additionally, gastroesophageal reflux was observed in three persons, and two individuals had early feeding difficulties requiring a nasogastric tube; of these, one individual needed a percutaneous endoscopic gastrostomy placement. Brain magnetic resonance imaging (MRI) of affected individuals from families 2, 3, and 5 did not detect structural abnormalities or myelination defects.

The protein-truncating variants identified in this study are expected to result in either reduced protein levels, due to degradation of mRNA via nonsense-mediated decay (NMD), or a truncated protein.[33,34] Accordingly, quantitative real-time PCR analysis showed that *EDEM3* mRNA levels in Epstein-Barr virus-transformed lymphoblastoid cell lines (EBV-LCLs) from affected individuals in family 1 were significantly decreased to 17% as compared to healthy controls ($p = 0.0078$; Figure 2A) and could be rescued with cycloheximide (CHX), an inhibitor of NMD, suggesting that the bi-allelic c.1859del frameshift variant triggers NMD. We repeated these experiments in fibroblasts from affected individuals in families 1 and 3 and confirmed that *EDEM3* is degraded to 18% of normal levels by NMD ($p = 0.0015$; Figure 2B). Immunoblots of EDEM3 were performed in two individual fibroblast cell lines from these two families. These demonstrated the absence of EDEM3 in individual IV-4 (family 1) and individual II-1 (family 3) consistent with loss of function of EDEM3 (Figure 3C). Because the function of EDEM3 could theoretically be compensated by EDEM1,[35] we quantified *EDEM1* (MIM: 607673) RNA levels in affected and control fibroblast cell lines. *EDEM1* levels were at 97% of normal levels ($p = 0.9373$) in fibroblast cell lines from affected individuals (Figure 2C). The comparable levels of *EDEM1* in affected and control fibroblast cell lines seems to suggest that *EDEM1* expression does not compensate for the reduction of *EDEM3* in these cells.

Previous studies have shown that EDEM3 belongs to a group of proteins that accelerate the degradation of misfolded glycoproteins in the ER. It is one of the ER 1,2-alpha mannosidases and specifically trims M8B to M7 (Figure 3A), which is then recognized by lectin OS-9 and targeted for degradation.[8–11] We hypothesized that loss of M8B to M7 trimming activity would result in

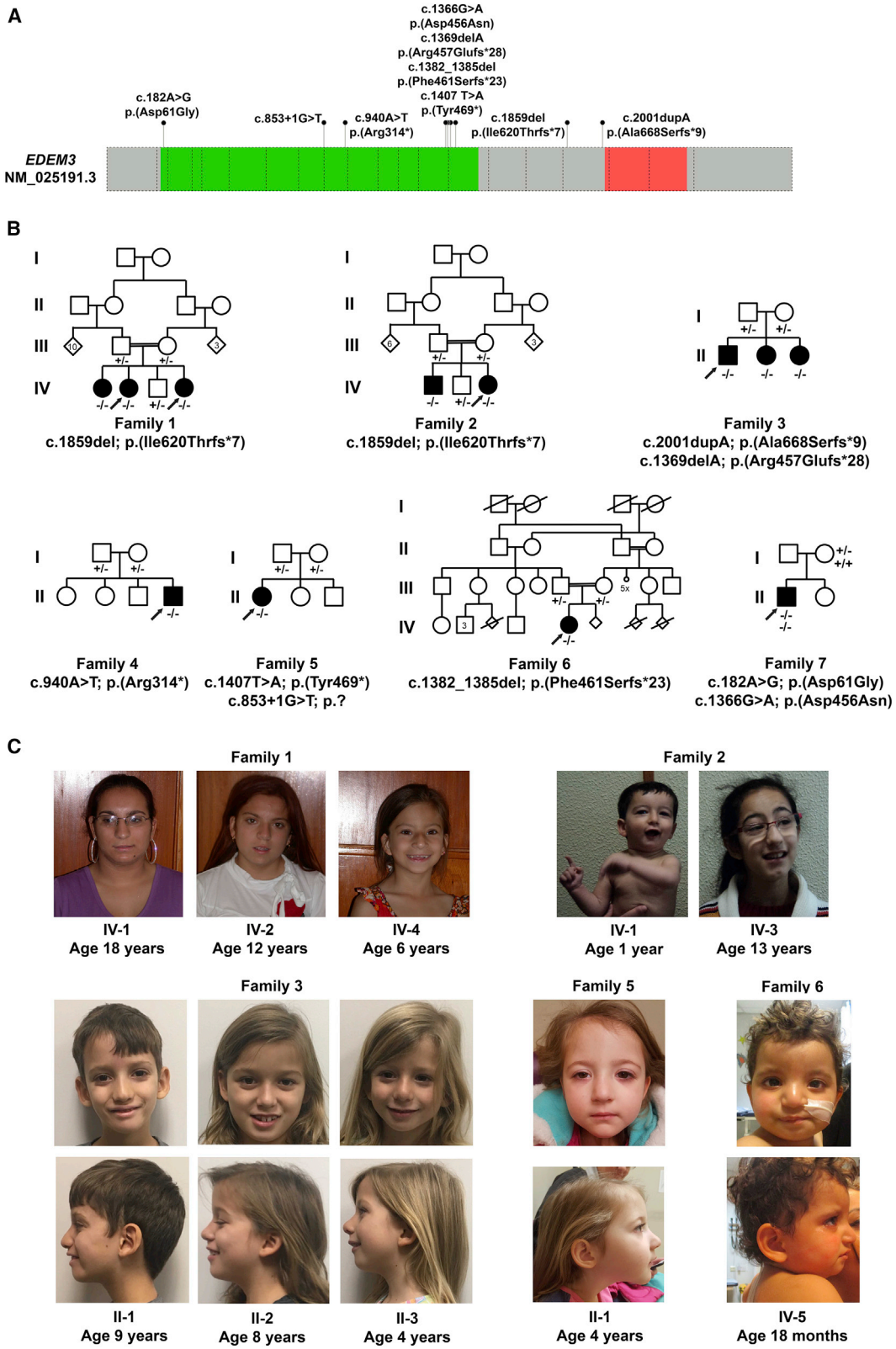

Figure 1. Bi-allelic variants in *EDEM3* lead to developmental delay or intellectual disabilities and dysmorphic features
(A) Schematic representation of human EDEM3 including the positions and the predicted effect on protein level of the seven identified variants in this study. The green box represents the Glyco_Hydro_47 domain, and the red box represents the protease-associated (PA) domain. Dashed boxes represent exons.
(B) Pedigrees of EDEM3-CDG families including the presence of the mutation. −, mutation present; +, wild-type.
(C) Craniofacial features of affected individuals, including narrow palpebral fissures, epicanthal folds, increased nasal height, bulbous nasal tip, hypoplastic alae nasi, short philtrum, thin upper lip, and retrognathia.

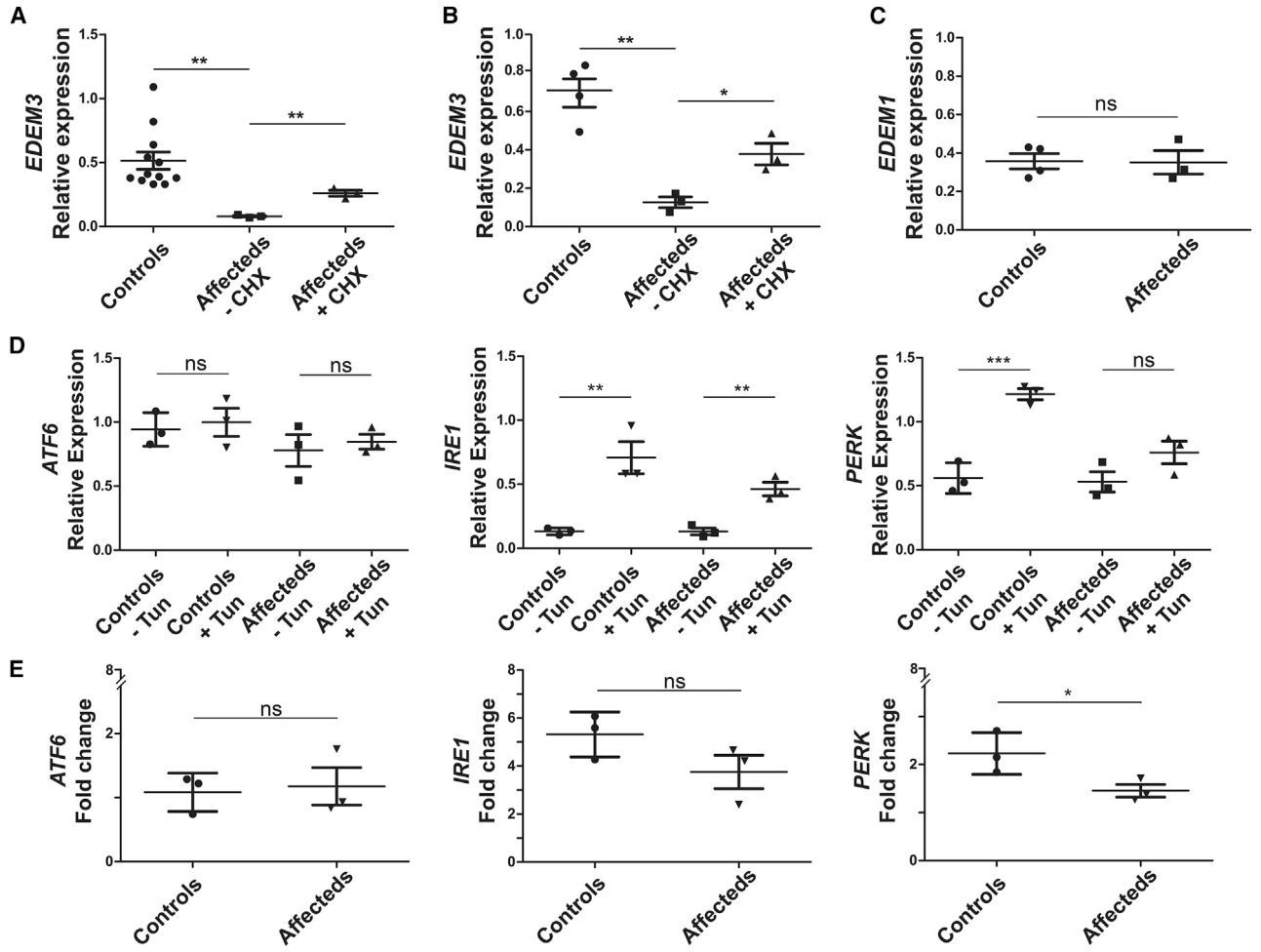

Figure 2. Relative expression of *EDEM3* mRNA and expression analysis of UPR markers

(A) A significant decrease of mRNA levels is seen between relative expressions of *EDEM3* in EBV-LCL from three affected individuals of family 1 with the bi-allelic c.1859del frameshift variant (n = 3) compared to healthy controls (n = 12; p = 0.0078) and samples treated with cycloheximide (CHX; n =3; p = 0.0016), normalized according to three housekeeping genes.

(B) *EDEM3* expression in fibroblast cell lines from family 1 (individual IV-4) and family 3 (individuals II-1 and II-2) confirming these results (p = 0.0015 and p = 0.0161 for CHX). Four controls were used.

(C) *EDEM1* expression in fibroblast cell lines from family 1 (individual IV-4) and family 3 (individuals II-1 and II-2) showing normal expression levels (p = 0.9373). Four controls were used.

(D) Analysis of total mRNA from EBV-LCL cell lines from controls revealed increased mRNA expression after treatment with tunicamycin (Tun) of *IRE1* and *EIF2AK3* (*PERK*) but not of *ATF6*.

(E) Affected individuals' mRNA from family 1 showed significantly decreased induction of *PERK* expression when compared to controls (p = 0.020), whereas *ATF6* and *IRE1* did not change significantly (p = 0.423 and p = 0.091, respectively). Experiments in (D) and (E) were performed with three control cell lines and three cell lines from affected individuals. Bars indicate mean values. Error bars represent standard deviation. ns, not significant; *p < 0.05; **p < 0.01; ***p < 0.001.

accumulation of abnormal N-glycans. Therefore, we determined the N-glycan profiles of total cellular glycoproteins prepared from a fibroblast cell line of a control individual and of an affected individual. Total N-glycan analysis via mass spectrometry in the affected individual's fibroblast cell line showed accumulation of M9 and M8 and reduced M7 and $Man_6GlcNAc_2$ (M6) levels (Figure S1). To study more precisely the impact of EDEM3 deficiency, we also analyzed the N-glycan profile after a pulse-chase experiment by using [2-^{3}H]mannose as precursor. We tested whether the variants in *EDEM3* affect the level of glycoproteins in fibroblast cell lines of individuals from families 1 and 3. In control fibroblast cells, we observed the anticipated levels of M8, M9, and $Glc_1Man_9GlcNAc_2$ (G1M9; Figure 3B). EDEM3 deficient cells from members of family 1 and 3 exhibited a similar pattern of N-glycan structures, although with increased accumulation of M5 and G1M5. The structure of these two species was confirmed with either saitoi or jack bean α-mannosidase treatment, as the G1M5 terminal glucose conferred substantial protection of the peak from the mannosidases (Figure S3). After 2 h of chase, the peaks for M7 and M4 did not appear in the cells of affected individuals (Figure 3B), indicating that the 1,2-alpha mannose residues were not removed from the M8B and M5 N-glycans during the chase, which is consistent with the absence of the biological function of

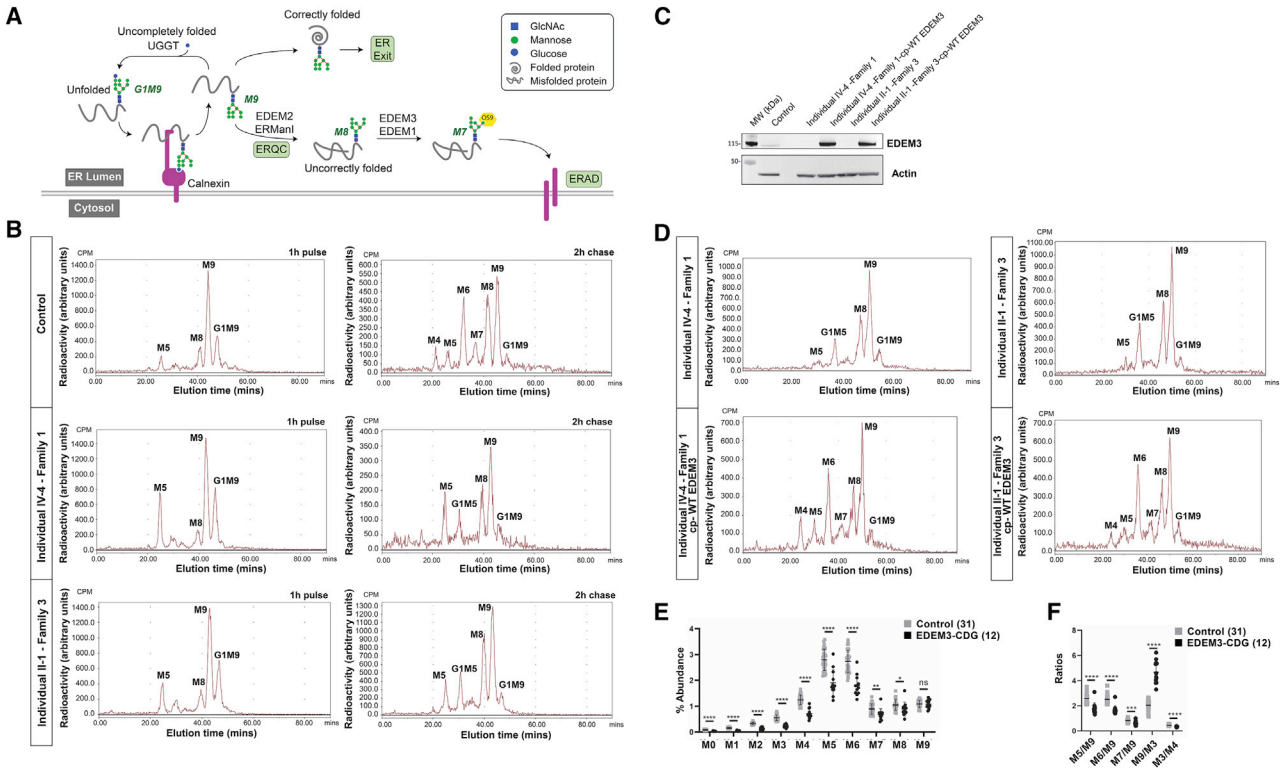

Figure 3. N-glycosylation pathway and N-glycan analysis of fibroblasts and plasma of human subjects

(A) N-glycosylaton pathway and the role of EDEM proteins in the mannose trimming and targeting for protein degradation in the cytosol.

(B) Accumulation of G1M5 and M5 and a lack of M7, M6, and M4 on newly synthesized N-glycoproteins in two EDEM3-CDG fibroblast cell lines from affected individuals. Fibroblasts from family 1 (individual IV-4) and family 3 (individual II-1) and one control individual were incubated with [2-^{3}H]mannose for 1 h and chased during 2 h.

(C) Immunoblot analysis of fibroblasts from individual IV-4 (family 1) and individual II-1 (family 3) before and after complementation with wild-type (WT) EDEM3. Total cell lysates were prepared and subjected to SDS-PAGE and immunoblot analysis with indicated antibodies.

(D) N-glycan analysis of fibroblasts from individual IV-4 and individual II-1 complemented with WT EDEM3 after incubation with [2-^{3}H] mannose for 1 h and chasing for 2 h.

(E) Percent abundance of plasma N-glycan species obtained from EDEM3-CDG-affected individuals and control individuals.

(F) Plot of ratio of plasma N-glycan species. Bars indicate mean values. Error bars represent standard deviation. Indicated p values from Student's t test, ns, not significant; *$p < 0.05$; **$p < 0.01$; ***$p < 0.001$; ****$p < 0.0001$.

EDEM3 (Figure 3A). We speculate that the M5 corresponds to the biosynthetic oligosaccharide precursor synthesized as a lipid-linked oligosaccharide and not generated through mannose trimming. The lipid-linked oligosaccharides profiles did not show M5 accumulation (data not shown). All together, these results may indicate that EDEM3 deficiency impairs lipid-linked oligosaccharide synthesis and that the M5 is transferred onto newly synthesized proteins and glucosylated to form G1M5 by the UDP-Glc:glycoprotein glucosyltransferase during calnexin cycle (Figure 3A).[36]

To evaluate the N-glycosylation of secreted glycoproteins, we studied the N-glycan profile of total plasma glycoproteins from all affected individuals, including the individual with compound heterozygous missense variants, by using our recently described and clinically validated semiquantitative N-glycan assay.[37] The N-glycan profiles from affected individuals showed decreased levels of low mannose N-glycan species M3–M7 (Figure 3C) with preserved normal M8 and M9 or sometimes mildly increased abundance of M9 as compared to control subjects. Ratios of the N-glycan abundances were also explored, and affected individuals had prominently decreased ratios of M5:M9, M6:M9, and M7:M9 as well as decreased M3:M4 (Figure 3D; Table S2). M6:M9 ratio provided the highest discrimination between tested obligate heterozygotes (parents, n = 4) and affected individuals (n = 12; Table S3). In theory, M3 can be produced by multiple pathways with or without EDEM3; thus, we used M9:M3 ratio to normalize M9 abundance. M9:M3 was increased in all 12 affected individuals. Stepwise ratio analysis for plasma N-linked polymannose species showed a reduction of M7:M8 that is significant in affected individuals, consistent with EDEM3's being the key enzyme in trimming M8B to M7 on secreted glycoproteins (Table S3).[9,10] Interestingly, M3:M4 ratio was also reduced in all 12 affected individuals tested, consistent with a possible role of EDEM3 in trimming M5 to shorter polymannose glycans, as suggested by the pulse

chase data. EDEM3's involvement in trimming of both M8 and M5 emphasizes that it is an essential ER mannosidase in humans. Of note, human transferrin was normally glycosylated in the common clinical screening test for CDG in the three affected individuals from family 3.

N-glycan profiles were also obtained from *Edem3* knockout (KO) mice (Figure S4). Although *Edem3* KO mice did not present with any obvious phenotype, subtle changes have been noted, such as reduced weight of brains and body and largely skewed ratios of homozygous KO pups versus heterozygous and wild-type pups. The profiles were acquired via a previously described method.[37] Similar to affected individuals, plasma from mice showed decreased ratios of M5:M9, M6:M9, and M7:M9 ($p < 0.02$; Figure S5B). In addition, mouse plasma proteins had significantly increased abundance of M8 and M9 ($p < 0.01$; Figure S5A). We also assayed mouse brain lysate for N-glycan profiles (Figure S5C) and ratios (Figure S5D). While plasma N-glycans reflect glycosylation of mature secreted glycoproteins and glycopeptides, N-glycan profiling of mouse tissue also includes cellular glycoproteins. Similar to mouse plasma N-glycan profiling, mouse brain showed increased high-mannose M8 and M9 N-glycan species (Figure S5C) and decreased ratios of M5:M9 and M6:M9 (Figure S5D).

N-glycan analysis of both *Edem3* KO mouse brain and plasma showed significant increases of the abundance M8 and M9. Thus, the known function of EDEM3 in trimming M8B is most likely shared by both humans and mice. In humans, not all the EDEM3-deficient individuals have increased M8 or M9 in the plasma. Instead, M9:M3 ratio is increased in all 12 affected individuals, providing a more sensitive diagnostic biomarker than M8 or M9 abundance in plasma. N-linked M3 and M4 are newly discovered small high-mannose species with low abundance on normal plasma glycoproteins.[37] Increases of M3 and M4 abundances have been reported as important diagnostic biomarkers for type I CDG subtypes, including PMM2-CDG, MPI-CDG, ALG3-CDG, and ALG9-CDG.[37–39] Significantly reduced abundance of N-linked M3 with a decreased M3:M4 ratio ($p < 0.0001$), however, has not been reported before. The reduction of M3 in all of the affected individuals suggests that a large portion of N-linked M3 in the control population is probably derived from glycan trimming ultimately involving human EDEM3 (Figure 3A). In the plasma from *Edem3* KO mice, M3:M4 ratio is not decreased (Figures S5B and S5D). Instead of increased M7:M8 ratio in humans, the increased M6:M7 ratio is the most significant, which may reflect a difference in overall substrate specificity between human and mouse EDEM3. The glycosylation abnormalities in both cellular or tissue proteins and secreted mature proteins indicate a global impact on protein N-glycosylation in EDEM3 deficiency. Consistent with our findings, it was previously demonstrated that EDEM3 participates in mannose trimming from total glycoproteins and not just misfolded proteins for ERAD.[10] Therefore, we propose this deficiency to be EDEM3-CDG.

The finding of abnormal N-glycan profiling pattern with reduced M3:M4, M5:M9, M6:M9, and M7:M9 ratios and increased M9:M3 among EDEM3-CDG-affected individuals provides additional diagnostic biomarkers for validating variants of uncertain significance, i.e., missense variants in *EDEM3*. One of the 12 EDEM3-CDG-affected individuals showed normal plasma of M5:M9 and M6:M9 ratios but also showed the lowest plasma N-linked M3:M4 ratio at 0.27 (normal 0.39–0.56) and a significantly increased M9:M3 ratio at 3.30 (normal 1.16–2.92) in this cohort. Therefore, the combination of high M9:M3 and low M3:M4 ratios might also provide diagnostic clues for EDEM3-CDG when M5:M9 and M6:M9 ratios are normal.

G1M5 accumulation is a marker for an impaired UPR.[36] Given the role of EDEM3 in gpERAD and its association with the UPR, we tested whether the UPR, a key quality-control process in the cell that is activated in response to the accumulation of misfolded proteins,[22] is affected in EDEM3-CDG. Quantitative real-time PCR analysis of total mRNA from EBV-LCLs from affected individuals showed decreased stimulation of *ERN1* (*IRE1* [MIM: 604033]) and *EIF2AK3* (*PERK* [MIM: 604032]) when cells were treated with tunicamycin, a UPR-inducing compound, as compared to controls (Figure 2D). *ATF6* (MIM: 605537) expression levels were similar. The difference in *IRE1* expression levels was not significant ($p = 0.091$), whereas the decreased stimulation of *PERK* expression levels in cell lines from affected individuals was significant ($p = 0.020$; Figure 2E), suggesting that the UPR is impaired in EDEM3-CDG or that these cell lines have an increased capacity to eliminate misfolded proteins.

EDEM3 was recently implicated in triglyceride metabolism. A low-frequency EDEM3 missense variant in the protease-associated domain (rs78444298, p.Pro746Ser, minor allele frequency ~1.5%) was associated with an approximately 5% decrease in triglyceride levels.[40] In our subjects for whom fasting triglyceride levels are available (Table S1), all triglyceride measurements were within the normal range. This most likely reflects the multiple metabolic pathways influencing triglyceride levels and makes the use of triglycerides as a diagnostic marker for EDEM3-CDG challenging.

In conclusion, we show that bi-allelic *EDEM3* variants cause EDEM3-CDG, a CDG with non-specific developmental delay and/or intellectual disability. Several affected individuals also have mild facial dysmorphisms. Given the increased accessibility of blood for clinical testing, semiquantitative N-glycan analysis provides additional diagnostic biomarkers for validating variants of uncertain significance that may be identified on molecular genetic testing. Further functional studies are necessary to determine the precise pathophysiological mechanism of EDEM3-CDG.

Data and code availability

All data that are relevant to this research are presented in this paper.

Supplemental information

Supplemental information can be found online at https://doi.org/10.1016/j.ajhg.2021.05.010.

Acknowledgments

We are grateful to the families that have participated to this study. This work was supported by the EU FP7 large-scale integrating project Genetic and Epigenetic Networks in Cognitive Dysfunction (241995) (to H.v.B.); National Institutes of Health (NIH) grants 5R01GM115730-03 (to M.H.), U54 NS115198 (to A.C.E. and M.H.), and T32GM008638 (to A.C.E.); and the Transatlantic Network of Excellence grant (10CVD03) from the Fondation Leducq and NIH NHGRI U01HG006398 (to D.J.R.). Family 4 was enrolled in the CAUSES Study; investigators include Shelin Adam, Christele Du Souich, Alison Elliott, Anna Lehman, Jill Mwenifumbo, Tanya Nelson, Clara Van Karnebeek, and Jan Friedman; it is funded by Mining for Miracles, British Columbia Children's Hospital Foundation (grant number F15-01355) and Genome British Columbia (grant number F16-02276). D.L.P. is recipient of a CAPES Fellowship (99999.013311/2013-01). X.B. is supported by an AHA career development award (19CDA34630032).

Declaration of interests

The authors declare no competing interests.

Consortia

The members of the CAUSES Study are Shelin Adam, Christele Du Souich, Alison Elliott, Anna Lehman, Jill Mwenifumbo, Tanya Nelson, Clara Van Karnebeek, and Jan Friedman.

Received: April 14, 2020
Accepted: May 19, 2021
Published: June 17, 2021

Web resources

gnomAD, https://gnomad.broadinstitute.org
OMIM, https://www.omim.org/

References

1. Brodsky, J.L. (2012). Cleaning up: ER-associated degradation to the rescue. Cell *151*, 1163–1167.
2. Needham, P.G., and Brodsky, J.L. (2013). How early studies on secreted and membrane protein quality control gave rise to the ER associated degradation (ERAD) pathway: the early history of ERAD. Biochim. Biophys. Acta *1833*, 2447–2457.
3. Smith, M.H., Ploegh, H.L., and Weissman, J.S. (2011). Road to ruin: targeting proteins for degradation in the endoplasmic reticulum. Science *334*, 1086–1090.
4. Thibault, G., and Ng, D.T.W. (2012). The endoplasmic reticulum-associated degradation pathways of budding yeast. Cold Spring Harb. Perspect. Biol. *4*, a013193.
5. Aebi, M., Bernasconi, R., Clerc, S., and Molinari, M. (2010). N-glycan structures: recognition and processing in the ER. Trends Biochem. Sci. *35*, 74–82.
6. Molinari, M. (2007). N-glycan structure dictates extension of protein folding or onset of disposal. Nat. Chem. Biol. *3*, 313–320.
7. Hosokawa, N., Tremblay, L.O., You, Z., Herscovics, A., Wada, I., and Nagata, K. (2003). Enhancement of endoplasmic reticulum (ER) degradation of misfolded Null Hong Kong alpha1-antitrypsin by human ER mannosidase I. J. Biol. Chem. *278*, 26287–26294.
8. Mast, S.W., Diekman, K., Karaveg, K., Davis, A., Sifers, R.N., and Moremen, K.W. (2005). Human EDEM2, a novel homolog of family 47 glycosidases, is involved in ER-associated degradation of glycoproteins. Glycobiology *15*, 421–436.
9. Ninagawa, S., Okada, T., Sumitomo, Y., Kamiya, Y., Kato, K., Horimoto, S., Ishikawa, T., Takeda, S., Sakuma, T., Yamamoto, T., and Mori, K. (2014). EDEM2 initiates mammalian glycoprotein ERAD by catalyzing the first mannose trimming step. J. Cell Biol. *206*, 347–356.
10. Hirao, K., Natsuka, Y., Tamura, T., Wada, I., Morito, D., Natsuka, S., Romero, P., Sleno, B., Tremblay, L.O., Herscovics, A., et al. (2006). EDEM3, a soluble EDEM homolog, enhances glycoprotein endoplasmic reticulum-associated degradation and mannose trimming. J. Biol. Chem. *281*, 9650–9658.
11. Hosokawa, N., Tremblay, L.O., Sleno, B., Kamiya, Y., Wada, I., Nagata, K., Kato, K., and Herscovics, A. (2010). EDEM1 accelerates the trimming of alpha1,2-linked mannose on the C branch of N-glycans. Glycobiology *20*, 567–575.
12. Olivari, S., Cali, T., Salo, K.E.H., Paganetti, P., Ruddock, L.W., and Molinari, M. (2006). EDEM1 regulates ER-associated degradation by accelerating de-mannosylation of folding-defective polypeptides and by inhibiting their covalent aggregation. Biochem. Biophys. Res. Commun. *349*, 1278–1284.
13. Hosokawa, N., Kamiya, Y., Kamiya, D., Kato, K., and Nagata, K. (2009). Human OS-9, a lectin required for glycoprotein endoplasmic reticulum-associated degradation, recognizes mannose-trimmed N-glycans. J. Biol. Chem. *284*, 17061–17068.
14. Fujita, E., Kouroku, Y., Isoai, A., Kumagai, H., Misutani, A., Matsuda, C., Hayashi, Y.K., and Momoi, T. (2007). Two endoplasmic reticulum-associated degradation (ERAD) systems for the novel variant of the mutant dysferlin: ubiquitin/proteasome ERAD(I) and autophagy/lysosome ERAD(II). Hum. Mol. Genet. *16*, 618–629.
15. Hirsch, C., Gauss, R., Horn, S.C., Neuber, O., and Sommer, T. (2009). The ubiquitylation machinery of the endoplasmic reticulum. Nature *458*, 453–460.
16. Rashid, H.-O., Yadav, R.K., Kim, H.-R., and Chae, H.-J. (2015). ER stress: Autophagy induction, inhibition and selection. Autophagy *11*, 1956–1977.
17. Guerriero, C.J., and Brodsky, J.L. (2012). The delicate balance between secreted protein folding and endoplasmic reticulum-associated degradation in human physiology. Physiol. Rev. *92*, 537–576.
18. Shang, J., Körner, C., Freeze, H., and Lehrman, M.A. (2002). Extension of lipid-linked oligosaccharides is a high-priority aspect of the unfolded protein response: endoplasmic reticulum stress in Type I congenital disorder of glycosylation fibroblasts. Glycobiology *12*, 307–317.
19. Lecca, M.R., Wagner, U., Patrignani, A., Berger, E.G., and Hennet, T. (2005). Genome-wide analysis of the unfolded protein response in fibroblasts from congenital disorders of glycosylation type-I patients. FASEB J. *19*, 240–242.
20. Yuste-Checa, P., Vega, A.I., Martín-Higueras, C., Medrano, C., Gámez, A., Desviat, L.R., Ugarte, M., Pérez-Cerdá, C., and Pérez, B. (2017). DPAGT1-CDG: Functional analysis of disease-causing pathogenic mutations and role of endoplasmic reticulum stress. PLoS ONE *12*, e0179456.

21. Walter, P., and Ron, D. (2011). The unfolded protein response: from stress pathway to homeostatic regulation. Science *334*, 1081–1086.
22. Ron, D., and Walter, P. (2007). Signal integration in the endoplasmic reticulum unfolded protein response. Nat. Rev. Mol. Cell Biol. *8*, 519–529.
23. Kim, I., Xu, W., and Reed, J.C. (2008). Cell death and endoplasmic reticulum stress: disease relevance and therapeutic opportunities. Nat. Rev. Drug Discov. *7*, 1013–1030.
24. Kimata, Y., and Kohno, K. (2011). Endoplasmic reticulum stress-sensing mechanisms in yeast and mammalian cells. Curr. Opin. Cell Biol. *23*, 135–142.
25. Termine, D.J., Moremen, K.W., and Sifers, R.N. (2009). The mammalian UPR boosts glycoprotein ERAD by suppressing the proteolytic downregulation of ER mannosidase I. J. Cell Sci. *122*, 976–984.
26. Xiang, C., Wang, Y., Zhang, H., and Han, F. (2017). The role of endoplasmic reticulum stress in neurodegenerative disease. Apoptosis *22*, 1–26.
27. Fribley, A., Zhang, K., and Kaufman, R.J. (2009). Regulation of apoptosis by the unfolded protein response. Methods Mol. Biol. *559*, 191–204.
28. Sano, R., and Reed, J.C. (2013). ER stress-induced cell death mechanisms. Biochim. Biophys. Acta *1833*, 3460–3470.
29. Tabas, I., and Ron, D. (2011). Integrating the mechanisms of apoptosis induced by endoplasmic reticulum stress. Nat. Cell Biol. *13*, 184–190.
30. Sobreira, N., Schiettecatte, F., Valle, D., and Hamosh, A. (2015). GeneMatcher: a matching tool for connecting investigators with an interest in the same gene. Hum. Mutat. *36*, 928–930.
31. Schwarz, J.M., Cooper, D.N., Schuelke, M., and Seelow, D. (2014). MutationTaster2: mutation prediction for the deep-sequencing age. Nat. Methods *11*, 361–362.
32. Sim, N.-L., Kumar, P., Hu, J., Henikoff, S., Schneider, G., and Ng, P.C. (2012). SIFT web server: predicting effects of amino acid substitutions on proteins. Nucleic Acids Res. *40*, W452-7.
33. Maquat, L.E. (1995). When cells stop making sense: effects of nonsense codons on RNA metabolism in vertebrate cells. RNA *1*, 453–465.
34. Baker, K.E., and Parker, R. (2004). Nonsense-mediated mRNA decay: terminating erroneous gene expression. Curr. Opin. Cell Biol. *16*, 293–299.
35. Shenkman, M., Ron, E., Yehuda, R., Benyair, R., Khalaila, I., and Lederkremer, G.Z. (2018). Mannosidase activity of EDEM1 and EDEM2 depends on an unfolded state of their glycoprotein substrates. Commun. Biol. *1*, 172.
36. Foulquier, F., Duvet, S., Klein, A., Mir, A.-M., Chirat, F., and Cacan, R. (2004). Endoplasmic reticulum-associated degradation of glycoproteins bearing Man5GlcNAc2 and Man9GlcNAc2 species in the MI8-5 CHO cell line. Eur. J. Biochem. *271*, 398–404.
37. Chen, J., Li, X., Edmondson, A., Meyers, G.D., Izumi, K., Ackermann, A.M., Morava, E., Ficicioglu, C., Bennett, M.J., and He, M. (2019). Increased Clinical Sensitivity and Specificity of Plasma Protein *N*-Glycan Profiling for Diagnosing Congenital Disorders of Glycosylation by Use of Flow Injection-Electrospray Ionization-Quadrupole Time-of-Flight Mass Spectrometry. Clin. Chem. *65*, 653–663.
38. Zhang, W., James, P.M., Ng, B.G., Li, X., Xia, B., Rong, J., Asif, G., Raymond, K., Jones, M.A., Hegde, M., et al. (2016). A Novel N-Tetrasaccharide in Patients with Congenital Disorders of Glycosylation, Including Asparagine-Linked Glycosylation Protein 1, Phosphomannomutase 2, and Mannose Phosphate Isomerase Deficiencies. Clin. Chem. *62*, 208–217.
39. Davis, K., Webster, D., Smith, C., Jackson, S., Sinasac, D., Seargeant, L., Wei, X.-C., Ferreira, P., Midgley, J., Foster, Y., et al. (2017). ALG9-CDG: New clinical case and review of the literature. Mol. Genet. Metab. Rep. *13*, 55–63.
40. Xu, Y.-X., Peloso, G.M., Nagai, T.H., Mizoguchi, T., Deik, A., Bullock, K., Lin, H., Musunuru, K., Yang, Q., Vasan, R.S., et al. (2020). EDEM3 Modulates Plasma Triglyceride Level through Its Regulation of LRP1 Expression. iScience *23*, 100973.

The American Journal of Human Genetics, Volume *108*

Supplemental information

Bi-allelic variants in the ER quality-control mannosidase gene *EDEM3* cause a congenital disorder of glycosylation

Daniel L. Polla, Andrew C. Edmondson, Sandrine Duvet, Michael E. March, Ana Berta Sousa, Anna Lehman, CAUSES Study, Dmitriy Niyazov, Fleur van Dijk, Serwet Demirdas, Marjon A. van Slegtenhorst, Anneke J.A. Kievit, Celine Schulz, Linlea Armstrong, Xin Bi, Daniel J. Rader, Kosuke Izumi, Elaine H. Zackai, Elisa de Franco, Paula Jorge, Sophie C. Huffels, Marina Hommersom, Sian Ellard, Dirk J. Lefeber, Avni Santani, Nicholas J. Hand, Hans van Bokhoven, Miao He, and Arjan P.M. de Brouwer

Figure S1. N-glycan analysis of fibroblasts from a control and an EDEM3 deficient individual.

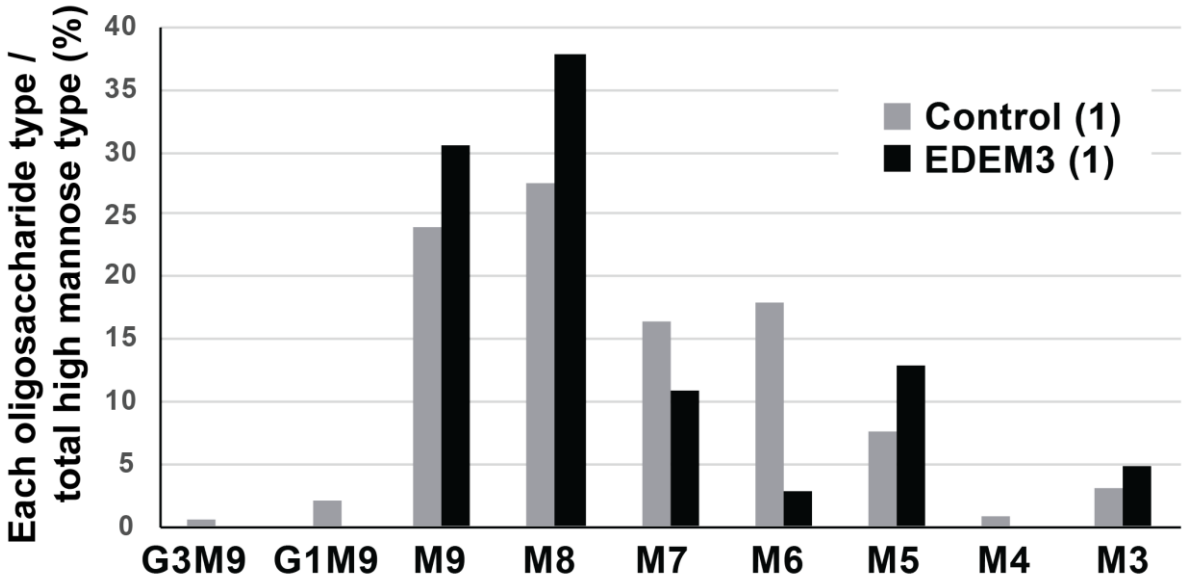

Mass spectrometry analysis of total N-glycans in fibroblasts from individual IV-2 of family 1 and a single control show accumulation of M9 and M8, and relatively lower M7 and M6 consistent with deficiency of EDEM3.

Figure S2. The representative N-glycan profiles of plasma from normal and EDEM3-CDG affected individuals.

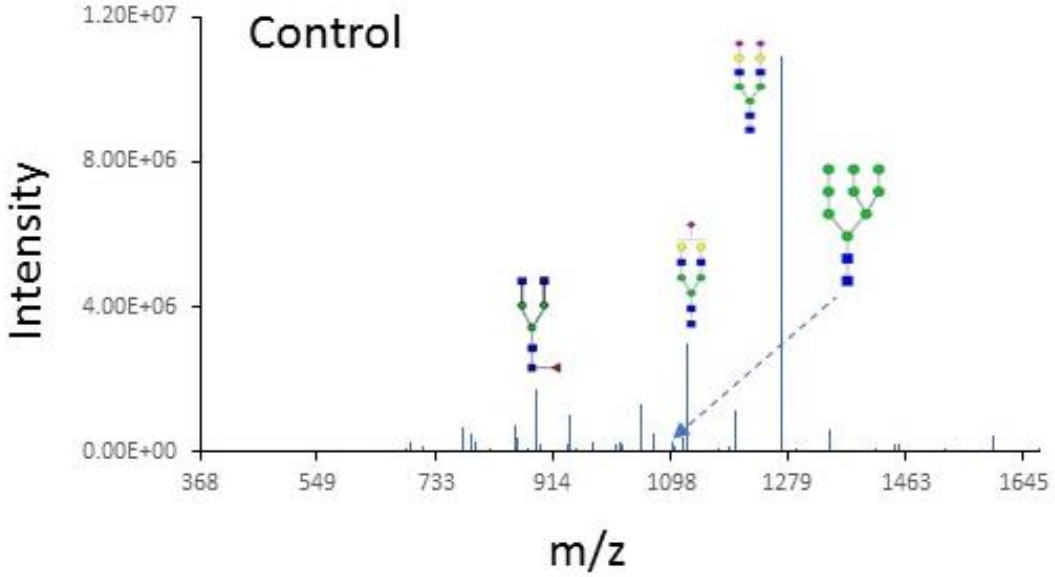

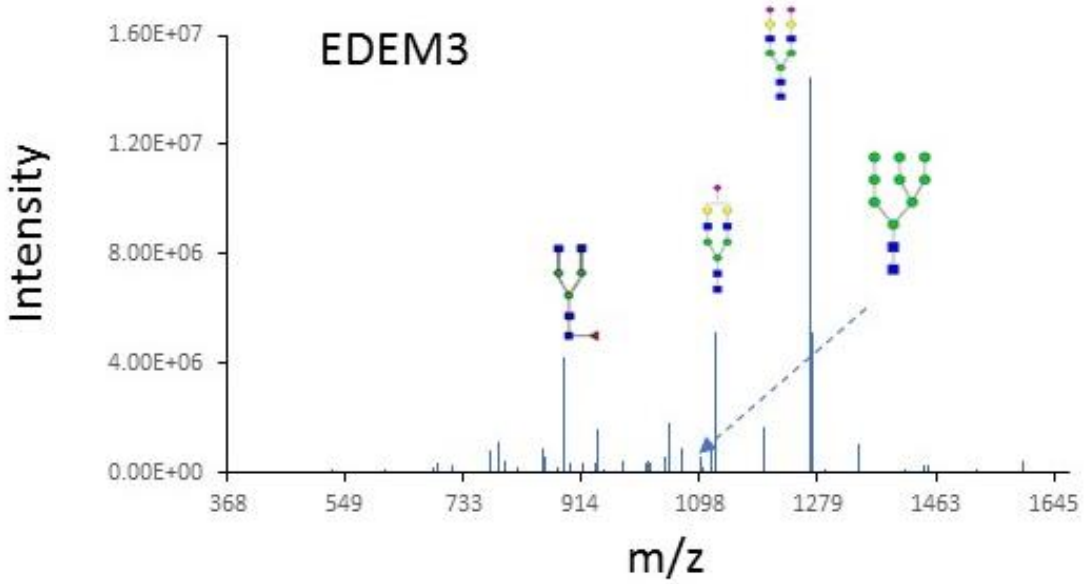

.
The overall abundance of complex glycans is normal in plasma EDEM3-CDG affected individuals.

Figure S3a. Characterization of the G1M5 structure in EDEM3 deficient cell lines.

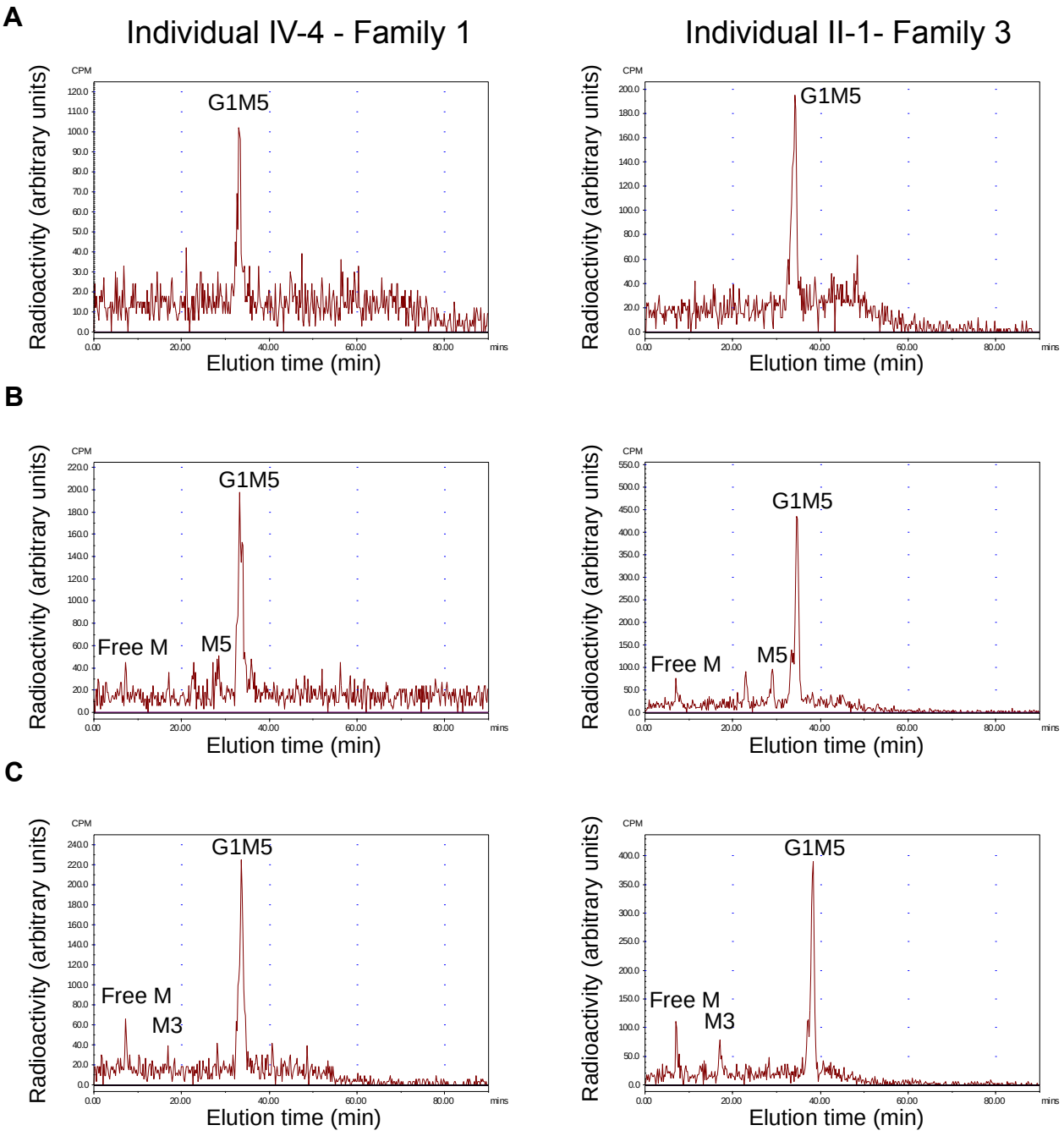

Patient fibroblasts from family 1 (individual IV-4) and family 3 (individual II-1) were incubated with [2-^{3}H] mannose for 1h and chased during 2h. A) HPLC profile of the G1M5 peak obtained from N-glycoproteins collected and isolated by HPLC analysis. B) HPLC profile of the isolated G1M5 after treatment with saitoi α1,2-mannosidase. C) HPLC profile of the isolated G1M5 peak after treatment with jack bean α-mannosidase. The G1M4 peak is not visible as jack bean α-mannosidase has difficulties in cleaving the α1,6-mannose residue after 2h. The M3, M5, and free M peaks are derived from M6, which is isolated together with the G1M5 peak.

Figure S3b. **Characterization of the M5 structure in EDEM3 deficient cell lines**.

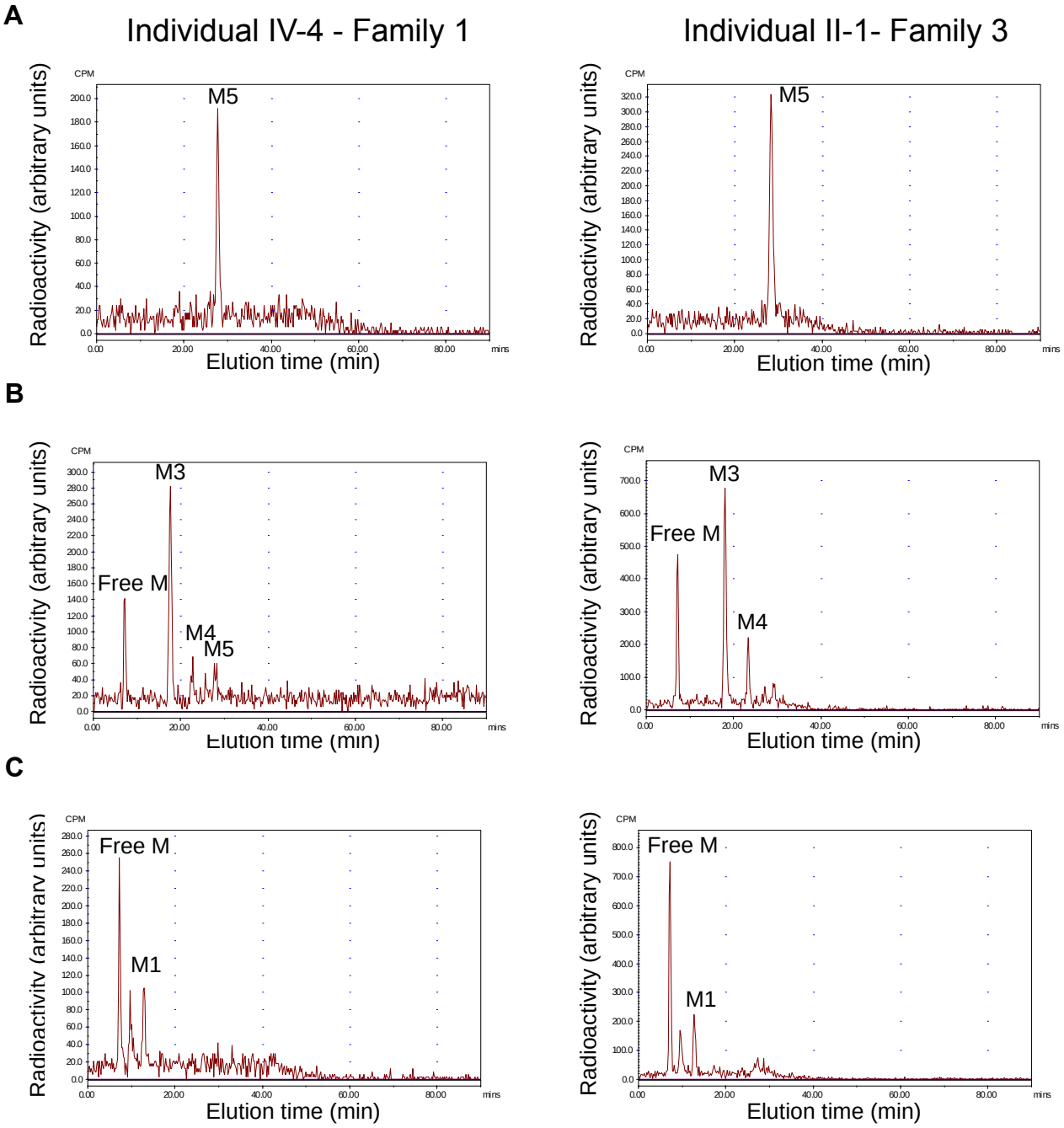

Patient fibroblasts from family 1 (individual IV-4) and family 3 (individual II-1) were incubated with [2-^{3}H] mannose for 1h and chased during 2h. A) HPLC profile of the M5 peak obtained from N-glycoproteins collected and isolated by HPLC analysis. B) HPLC profile of the isolated M5 after treatment with saitoi α1,2-mannosidase. C) HPLC profile of the isolated M5 peak after treatment with jack bean α-mannosidase

Figure S4. Deletion of 47bp in mouse *Edem3* exon 3 results in a protein null.

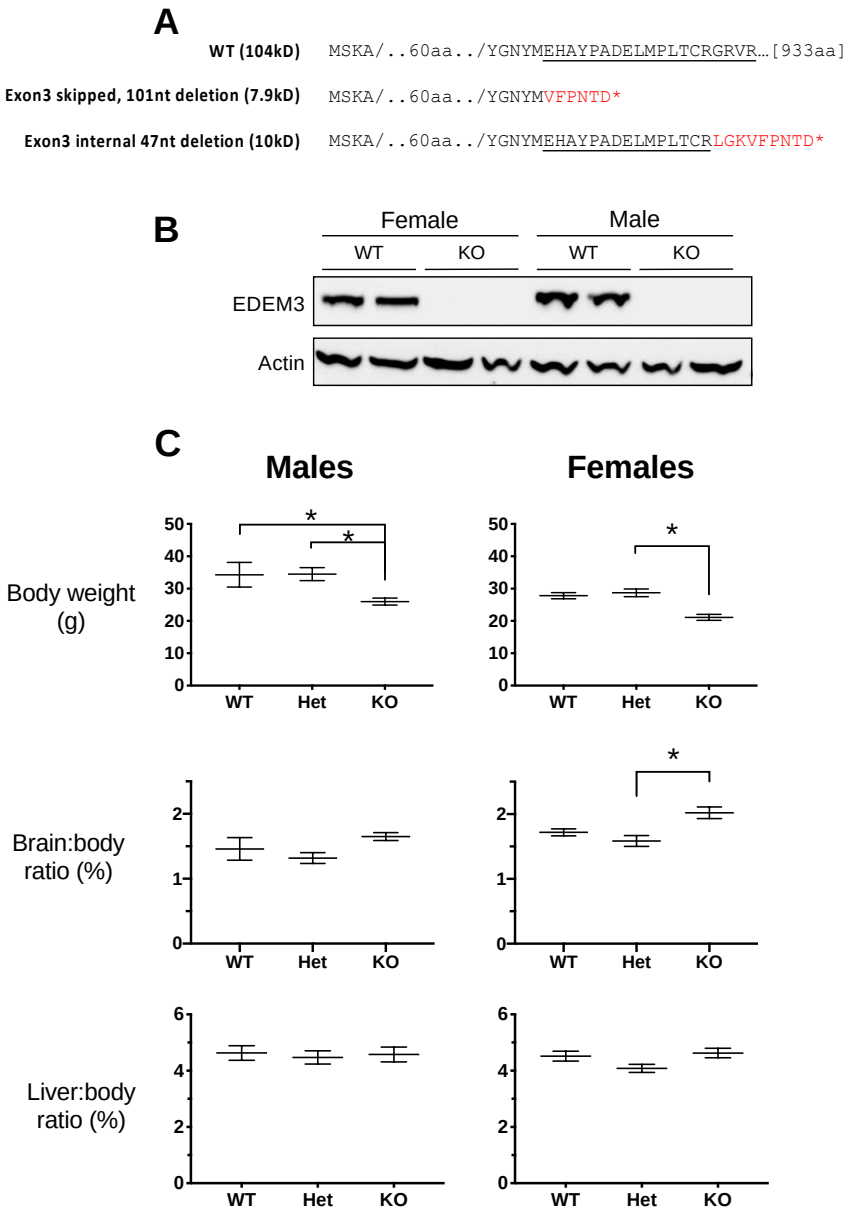

A) Predicted polypeptide sequences from splice variants detected in liver from homozygous *Edem3* KO mice, either with *Edem3* exon 3 skipped, or the exon 3 with in a internal 47bp deletion (*Edem3* KO allele), relative to the reference transcript (WT). Underlined text=exon 3 (partial sequence); red text=frameshifted sequence. B) Western blot using a polyclonal rabbit antibody against EDEM3 of 100µg of protein from control or *Edem3* KO mouse liver lysate. Two wildtype females and two wildtype males are compared with two knock-out females and two knock-out males showing that there is no expression of Edem3 protein in the liver of knock-out animals. C) Body weight, brain weight adjusted to body weight (expressed as a percentage), and liver weight adjusted to body weight (expressed as a percentage) of male and female mice is given. Wild-type (WT), heterozygous (Het), or knockout (KO) for *Edem3* aged between 52 and 80 weeks at time of sac are shown. The age of the mice did not differ significantly between genotypes in either sex. The body weight of the KO mice was significantly lower than that of heterzygous mice in both sexes, and that of WT male mice, suggesting a mild kachexia phenotype. Brain to body weight in female KO was modestly but significantly increased. One-way ANOVA, Tukey's multiple comparison test, *P<0.05. Male mice: WT n=5; Heterozygous n=4; KO n=6. Female mice: WT n=6; Het n=13; KO n=4.

Figure S5. N-glycan analysis of *Edem3* KO and WT mice.

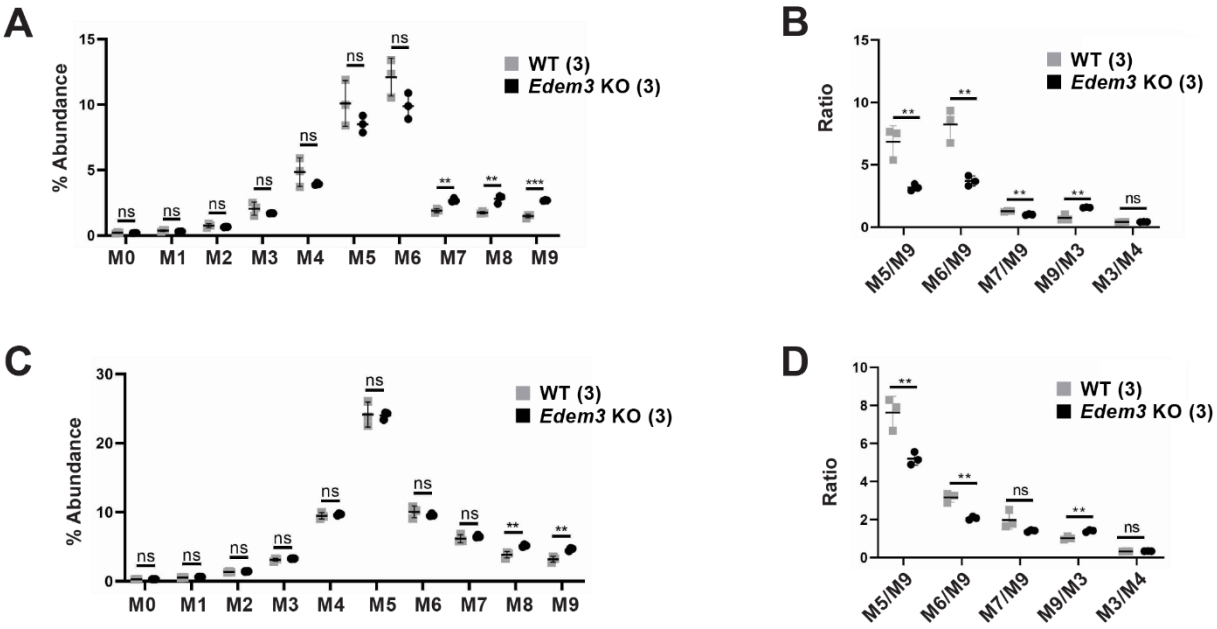

A) Abundance of murine plasma n-glycan species. B) Ratio of murine plasma n-glycan species. C) Abundance of murine brain n-glycan species. D) Ratio of murine brain n-glycan species. Bars indicate mean values. Error bars represent standard deviation. Indicated P-values from Student's T-test, ns = not significant; **P*<0.05; ***P*<0.01; ****P*<0.001.

Supplemental material and methods

Exome Sequencing (ES), Filtering, and Annotation

High-throughput sequencing was performed for sibling pairs of families 1 and 2 at BGI (BGI-Shenzhen, Shenzhen, China). Exome capturing was carried out by using Agilent SureSelect Target Enrichment V5 (Agilent Technologies, Santa Clara, CA, USA). Sequencing was performed by using the Illumina HiSeq 2000 platform (Illumina, San Diego, CA, USA). Illumina base calling software v1.7 was employed to analyze the raw image files with default parameters. Data analysis was performed using the Roche Newbler software (v.2.3) using human genome build hg19/GRCh37. Selection of the variants was performed by using a seven tier filtering strategy as previously described [1]. Potential causative variants found by ES were confirmed by Sanger sequencing. Primers were designed by using the online software Primer3plus [2]. Amplifications were performed using standard methods. PCR products were visualized by gel electrophoresis. Subsequently, enzymatic DNA purification with ExoI (New England BioLabs, Ipswich, MA, USA) and Fast AP (ThermoFischer Scientific, Waltham, MA, USA) was carried out using a thermal cycler starting with incubation at 37 °C for 15 minutes followed by an additional 15 minutes incubation at 80 °C. PCR products were sequenced using the ABI PRISM BigDye Terminator Cycle Sequencing V2.0 Ready Reaction Kit and analyzed with the ABI PRISM 3730 DNA analyzer (Applied Biosystems, Foster City, CA, USA).

ES for family 3 was performed as a trio with patient 6 and his parents at the Children's Hospital of Philadelphia. Exome capture was performed using the Agilent SureSelect XT Clinical Research Exome kit per manufacturer's protocol (Agilent Technologies, Santa Clara, CA, USA) and sequenced on the Illumina HiSeq 2000 or 2500 platform with 100bp paired-end reads (Illumina, San Diego, CA, USA). Mapping and analysis were based on the human genome build UCSC hg19 reference sequence. Potential causative variants found by ES were confirmed by Sanger sequencing as was the presence of the *EDEM3* variants in affected siblings, patients 7 and 8. Read alignment and variant calling were performed with an in-house bioinformatics pipeline incorporating NovoAlign (Novocraft, Selangor, Malaysia,

http://www.novocraft.com/) for read alignment; Picard (Broad Institute, Cambridge, MA) for marking duplicates; and Genome Analysis Toolkit's (GATK) (Broad Institute, Cambridge, MA) [3,4]. Best Practices for UnifiedGenotyper, with no parameter modifications, for variant calling (reference sequence: hg19/GRCh37) and variant filtering based on read depth (≥5X). Variant filtration was performed with an in-house bioinformatics pipeline. Analysis was performed as previously described [5].

Family 4 underwent trio exome sequencing at Ambry Genetics (Aliso Viejo, CA, US) as part of a research contract in a study protocol (H15-00092) approved by the University of British Columbia. Coding regions were captured with IDT xGen Exome Research Panel v1.0 (Coralville, IA, US). Sequencing on an Illumina (San Diego, CA, USA) platform was performed to the depth such that 99% of consensus coding regions were sequenced at least 10X. Alignment of 150bp reads to the reference genome (GRCh37/Hg19) and variant calling was performed with BWA-MEM (35), GATK, SAMtools, and Picard, and then annotated and prioritized with VarSeq v.1.5 (Golden Helix, Bozeman, MT, US) [3].

For family 5, the patient's genomic DNA was analyzed in comparison with the published human genome build GRCh37/hg19. Using a custom-developed analysis tool (XomeAnalyzer; GeneDx, Gaithersburg, MD, USA), data were filtered and analyzed to identify sequence variants and most deletions and duplications involving three or more coding exons [6]. Reported clinically significant variants were confirmed by an appropriate orthogonal method in the proband and in selected relatives as necessary. Sequence and copy number variants are reported according to the Human Genome Variation Society (HGVS) or International System for Human Cytogenetic Nomenclature (ISCN) guidelines, respectively.

Trio exome sequencing was performed for family 6 using the Twist Human Core Exome Kit (Twist Bioscience, San Francisco, CA, USA). Sequencing of paired-end 150bp reads was performed on a NextSeq500 (Illumina, SanDiego, CA, USA). BWA-MEM (v0.7.12) [7] was used to de-multiplex and align Illumina NextSeq FASTQ reads to the reference genome (GRCh37/Hg19). After conversion to BAM file format and duplicate removal (Picard v1.129; http://broadinstitute.github.io/picard/), indel realignment, variant calling and quality filtering was

performed using GATK (v3.4-46) [3]. Variant annotation was performed using Alamut Batch (Interactive Biosoftware, Rouen, France) and variant filtering was performed as previously described [8,9].

Duo exome capturing was carried out for family 7 by using Agilent SureSelect Target Enrichment Clinical Research Exome V2 (Agilent Technologies, Santa Clara, CA, USA). Sequencing (paired-end 150bp) was performed by the Illumina HiSeq 4000 platform (Illumina, San Diego, CA, USA). Data was demultiplexed by Illumina Software CASAVA. Reads are mapped to the genome (hg19/GRCh37) with the program BWA (http://bio-bwa.sourceforge.net/). Variants are detected with the Genome Analysis Toolkit (http://www.broadinstitute.org/gatk/). Subsequently, variants were filtered with the Alissa Interpret software package (Agilent Technologies, Santa Clara, CA, USA) and were further selected based on two inheritance models (autosomal recessive and X-linked recessive/dominant).

Cell lines and culture maintenance

Epstein-Barr-virus-transformed lymphoblastoid (EBV-LCL) cell lines derived from patients and fibroblast cell lines were grown in Dulbecco's Modified Eagle Medium (DMEM) supplemented with 10% (volume/volume) fetal calf serum (catalog no. F7524; Sigma Aldrich, St. Louis, MO, USA), 1% (volume/volume) sodium pyruvate (catalog no. S8636; Sigma Aldrich, St. Louis, MO, USA), and penicillin/streptomycin (catalog no. P4333; Sigma Aldrich, St. Louis, MO, USA). To analyze the effect of nonsense-mediated mRNA decay (NMD) on the gene expression, 1 µg/ml cycloheximide (C4859-1 ml; Sigma Aldrich, St. Louis, MO, USA), an inhibitor of NMD, is used to inhibit degradation of nonsense RNA in five fibroblasts lines for 4 hours. To analyze the potential effect on the cellular stress response mechanism, 4 µg/ml tunicamycin (catalog no. T7765-5MG; Sigma Aldrich, St. Louis, MO, USA) was used to induce stress in three control and three EBV-LCL lines, and six controls and six fibroblasts lines for 5 hours after which the cells were harvested [10,11].

RNA isolation, cDNA Synthesis and quantitative real time PCR (qPCR)

All RNA isolations were performed with the NucleoSpin RNA Clean-up Kit (catalog no. 740955-50, Macherey-Nagel, Düren, Germany) according to manufacturer's protocol. RNA was quantified by NanoDrop (Thermo Fisher Scientific, Waltham, MA, USA). Considering that the mutations are predicted to trigger NMD, we examined the expression level of *EDEM3* mRNA using qPCR analysis. Total RNA was isolated from EBV-LCL from the proband and two affected siblings of family 1, and fibroblast cell lines of individual IV-4 from family 1 and of individuals II-1 and II-2 from family 3 with or without cycloheximide (CHX). For qPCR, 2 µg total RNA was reverse transcribed into cDNA using the SuperScript VILO Master Mix (catalog no. 11755050, Thermo Fisher Scientific, Waltham, MA, USA), following manufacturer's instructions. Amplifications were performed in duplicates of 25 µl reactions in the presence of SYBR green (Applied Biosystems, Foster City, CA, USA), using the absolute quantification setting on an ABI PRISM 7900HT Sequence Detection System (Applied Biosystems, Foster City, CA, USA), using the ΔΔCt method, as described before [12], to quantify differences in gene expression compared to housekeeping genes *GUSB*, *PPIB* and *CLK2*. Additionally, to test the potential effect of the *EDEM3* mutations in the UPR stress response of the cells [10,11], qPCR analysis was performed using primers located in the *IRE1*, *ATF6* and *PERK* genes, in cDNA collected from EBV-LCL cells derived from three affected family members and three healthy EBV-LCL controls; all treated with and without tunicamycin. Results were analyzed using the ΔΔCt method described previously[12,13]. Primer sequences are available upon request.

Antibodies and Western blot analysis

Anti-EDEM3 antibodies were purchased from Signalway Antibody LLC (Maryland, USA), anti-β-actin antibodies from MilliporeSigma (Burlington, MA, USA), and goat anti-rabbit or goat anti-mouse immunoglobins conjugated to h*orseradish peroxidase* (HRP) were ordered from Agilent Technologies (Santa Clara, CA, USA). Cells were pelleted and lysed in RIPA Buffer (50 mM Tris-HCl pH 7.9, 120 mM NaCl, 1% NP40, 1 mM EDTA, 1 mM Na_3VO_4, 55 mM NaF) supplemented with a cocktail of protease inhibitors (Roche, Meylan, France). Cells were

centrifuged at 20,000g and 4°C for 10 min. The protein concentration contained in the supernatant was determined with a MicroBCA™ Protein Assay Reagent kit (Thermo Fisher Scientific, Waltham, MA USA). Twenty micrograms of total protein of each sample were dissolved in reducing NuPage Sample buffer and separated on 4-12% Bis-Tris gel (Thermo Fisher Scientific, Waltham, MA, USA) and transferred to nitrocellulose membranes Hybond ECL (GE Healthcare, Little Chalfont, UK). Membranes were blocked using Tris-buffered saline (TBS) containing 0.05% Tween20 and 5% (w/v) bovine serum albumin (BSA). Primary antibodies rabbit anti-EDEM3 and mouse anti-actin (for quantification) were incubated overnight at 4°C in TBS, 0.05% Tween20 (TBS-T) and 5% (w/v) BSA at respectively 1:500 and 1:10,000 dilution. Menbranes were washes three times 5 min in TBS-T after addition of the primary and secondary antibodies. Either goat anti-rabbit IgG and goat anti-mouse IgG HRP conjugated were used as secondary antibodies at dilution of 1:5,000 and 1:20,000. Signal was detected by a chemilescence reagent (PierceTM Pico Plus Westernblotting Substrate ; Thermo Fisher Scientific, Waltham, MA, USA) on a imagin film (GEHealthcare, Buckinghamshire, UK).

Alpha-mannosidase treatment of N-glycans

N-glycans were incubated in 200 µL 50 mM ammonium acetate buffer pH 4.5 with 0.5 U of jack bean α-mannosidase (EC 3.2.1.24, Sigma Aldrich, St. Louis, MO, USA) or in 200 µL of 20 mM sodium acetate buffer pH 5 with 0.5 U of α1,2-mannosidase (EC 3.2.1.113, isolated from Aspergillus saitoi, Glyko, UK). Enzyme digestions were carried out at 37 °C for 24 h with a fresh aliquot of enzyme added after 16 h. Released glycans were then analysed by HPLC.

Development of a novel mouse model of Edem3 genetic deficiency

A mouse model of *Edem3* genetic deficiency was generated at the Transgenic and Chimeric Mouse Facility of the University of Pennsylvania, by coinjection into fertilized C57BL6/J zygotes of spCas9 mRNA (TriLink Biotechnologies, San Diego, CA), along with RNA oligos corresponding to tracrRNA and two separate *Edem3* guide RNAs (GR5, 5'-GCCUCUGACACGGCCCCGGC and GR6, 5'-GGGCGAUGUGGAUGACGCCU; Integrated

DNA Technologies, Coralville, IA). Founder mice with biallelic deletion of a 47bp DNA sequence between the GR5 and GR6 gRNA target sequences, were identified by PCR of genomic DNA, and confirmed by Sanger sequencing. The deleted sequence (GGGGCCGTGTCAGAGGCCAGGAGCCCAGCCGGGGCGATGTGGATGAC) results in a frameshift deletion within *Edem3* exon 3 (which is present in all predicted *Edem3* transcripts). Liver RNA was reverse transcribed, and a region of *Edem3* cDNA was amplified with transcript-specific primers (mmEDEM3F376, 5'-TGATCATGCTT-ATGGCAACTATATG and mmEDEM3R822 5'-AACTTTAAATTAATCCTGGGGTACG). PCR products were cloned by TopoTA cloning, and Sanger sequencing demonstrated the presence of two transcript variants, the first of these confirmed transcription of the deleted DNA, while the second revealed a novel splice variant in which the partially deleted exon 3 was skipped, with direct splicing of exon 2 to exon 4 (leading to a 101 nucleotide deletion relative to the reference transcript). Importantly, both of these splice variants lead to early frameshifts, Arg84fs*9 in the case of the 47nt deletion, and Met69fs*5 for the exon2-exon4 splice variant. The biallelic 47bp deletion was confirmed to result in a protein null by Western blot of liver lysate with a rabbit polyclonal directed against a conserved C-terminal region (amino acids 854-903 of Human EDEM3 protein according to Q9BZQ6; ab118762, Abcam, Boston, MA). These data are summarized in **Supplemental Figure S3.**

While the biallelic 47bp deletion was compatible with life, and the escaping *Edem3* knockout (KO) mice had no overt phenotypes, we note that *Edem3* KO pups were consistently recovered at considerably lower than the expected Mendelian ratio, suggesting that there is a strong development selection for EDEM3 function. *Edem3* KO females crossed to an *Edem3* heterozygous male produced 4.8% KO pups (expected 50%, P <0.0001), the reciprocal cross (KO male crossed to heterozygous females) yielded KO pups at 8.8% (expected 50%, P <0.0001), and heterozygous male to heterozygous females generated 1.7% KO pups (expected 25%, P =0.0002).

Culturing of fibroblasts

All fibroblasts were cultured in high glucose DMEM (D0819, Sigma-Aldrich) supplemented with 20% fetal calf serum (FCS; F7524, Sigma-Aldrich), 1% penicillin/streptomycin (P/S; P4333, Sigma-Aldrich) and 1% sodium pyruvate (S8636, Sigma-Aldrich). Fibroblasts were incubated at 37°C/5% CO_2. After transduction fibroblasts were cultured in the same conditions, with medium supplemented with 0.5 µg/ml puromycin (P9620; Sigma-Aldrich).

Transduction of patient fibroblasts with hEDEM3

Lentiviral constructs with hEDEM3 (NM_001319960.2) driven by a human cytomegalovirus (CMV) promoter and with a puromycin resistance gene were constructed and generated by VectorBuilder (>10^8 TU/ml in Hanks' Balanced Salt solution; HBSS buffer). An enhanced green fluorescent (eGFP) control lentivirus (VB160109-10005, VectorBuilder) was used to control for transduction efficiency. Patient fibroblasts were seeded at a density of 10^5 cell per well of a 6-well plate (353046, Corning) the day before transduction. Transduction was done overnight in medium supplemented with 5 µg/ml polybrene (VectorBuilder). Two days after transduction, selection of transduced cells was started with increasing concentrations of puromycin (0.5 µg/ml – 2 µg/ml).

N-glycan profiling of cultured skin fibroblasts

Fibroblasts of a healthy control and of EDEM3-CDG individual IV-2 of family 1 (about 10 million of cells) were harvested by scraping. Protein denaturation and N-glycan release were performed according to Abu Bakar *et al* [14]. Released N-glycans were purified and enriched using graphitized carbon cartridges and N-glycans were eluted using 40% acetonitrile and 0.05% trifluoroacetic acid. Mass spectrometry analysis of total fibroblast N-glycans was performed using a porous graphitized carbon (PGC) chip on an Agilent 1260 Infinity HPLC-chip on an Agilent 6540 QTOF mass spectrometer (Agilent Technologies, Santa Clara, CA,

USA). MS data were analyzed using Agilent Mass Hunter Qualitative Analysis Software. Relative glycan abundances were calculated as described before [15].

Pulse-chase labeling analysis of N-glycans in cultured human fibroblasts

Fibroblast cell lines were preincubated at 0.5 mM glucose for 45 min and then metabolically labeled for 1h with 3.7 MBq/mL (2.25 μM) [2-3H] mannose at the same glucose concentration. When a chase was performed, pulse-labeled cells were washed twice with phosphate-buffered saline pH 7.4 (PBS) and incubated for 2h in DMEM medium containing 5 mM glucose. Sequential extraction and purification of oligosaccharide material were performed as described previously [16]. The protein pellet was digested overnight at room temperature with trypsin (1 mg/mL) in 0.1 M of ammonium bicarbonate buffer, pH 7.9. Subsequently, glycopeptides were treated overnight at 37°C with 0.5 U PNGase F in a 50 mM phosphate buffer, pH 7.2, to release oligosaccharides. The oligosaccharide fractions were then desalted on Bio-Gel P2 with 5% acetic acid. The analysis of the oligosaccharides was performed by high-performance liquid chromatography (HPLC) on an amino-derivatized Asahipak NH2P-50 column (250 mm×4.6 mm; Asahi, Kawasaki-Ku, Japan) with an acetonitrile/water gradient from 70:30 (v/v) to 50:50 (v/v) at a flow rate of 1 mL/min over 90 min. Elution of the radiolabeled oligosaccharides was monitored by continuous-flow detection of the radioactivity with a flo-one detector (Perkin-Elmer, Les Ullis, France).

Semi-quantitative analysis of N-glycans in human and mouse plasma and mouse brain tissue

N-glycans were prepared from heparinized plasma and analyzed as previously described **[17]**. Briefly, plasma samples were combined with internal standard of [^{13}C]-sialylglycopeptide, digested with Rapid PNGase FTM, reacted with RapiFluor-MS reagent, and subsequently flow injected and analyzed with a Waters Synapt G2 Si electrospray-ionisation quadrupole time-of-flight mass spectrometry (ESi-QTOF) in positive ion mode. For N-glycan analysis on mouse brain, whole brain was lysed in water by sonication and lysate of 200 μg of protein was subject to PNGaseF digestion and N-glycan analysis as described above.

Statistical testing

After log transformation, differences in gene expression by qPCR were tested with a student's t-test in excel. Student's t-test to measure the difference between the means in two independent samples was also used to analyze N-glycan performing pairwise comparisons of each glycan. Level of significance was uncorrected for multiple testing and set at $P \leq 0.05$.

References

1. Riazuddin, S., Hussain, M., Razzaq, A., Iqbal, Z., Shahzad, M., Polla, D.L., Song, Y., van Beusekom, E., Khan, A.A., and Tomas-Roca, L. (2016). Exome sequencing of Pakistani consanguineous families identifies 30 novel candidate genes for recessive intellectual disability. Mol. Psychiatry.

2. Untergasser, A., Cutcutache, I., Koressaar, T., Ye, J., Faircloth, B.C., Remm, M., and Rozen, S.G. (2012). Primer3--new capabilities and interfaces. Nucleic Acids Res *40*, e115.

3. Van der Auwera, G.A., Carneiro, M.O., Hartl, C., Poplin, R., Del Angel, G., Levy-Moonshine, A., Jordan, T., Shakir, K., Roazen, D., Thibault, J., et al. (2013). From FastQ data to high confidence variant calls: the Genome Analysis Toolkit best practices pipeline. Curr. Protoc. Bioinforma. *43*, 11.10.1-33.

4. McKenna, A., Hanna, M., Banks, E., Sivachenko, A., Cibulskis, K., Kernytsky, A., Garimella, K., Altshuler, D., Gabriel, S., Daly, M., et al. (2010). The Genome Analysis Toolkit: A MapReduce framework for analyzing next-generation DNA sequencing data. Genome Res. *20*, 1297–1303.

5. Gibson, K.M., Nesbitt, A., Cao, K., Yu, Z., Denenberg, E., DeChene, E., Guan, Q., Bhoj, E., Zhou, X., Zhang, B., et al. (2018). Novel findings with reassessment of exome data: implications for validation testing and interpretation of genomic data. Genet. Med. Off. J. Am. Coll. Med. Genet. *20*, 329–336.

6. Retterer, K., Scuffins, J., Schmidt, D., Lewis, R., Pineda-Alvarez, D., Stafford, A., Schmidt, L., Warren, S., Gibellini, F., Kondakova, A., et al. (2015). Assessing copy number from exome sequencing and exome array CGH based on CNV spectrum in a large clinical cohort. Genet. Med. Off. J. Am. Coll. Med. Genet. *17*, 623–629.

7. Li, H., and Durbin, R. (2009). Fast and accurate short read alignment with Burrows-Wheeler transform. Bioinforma. Oxf. Engl. *25*, 1754–1760.

8. Allen, H.L., Flanagan, S.E., Shaw-Smith, C., De Franco, E., Akerman, I., Caswell, R., International Pancreatic Agenesis Consortium, Ferrer, J., Hattersley, A.T., and Ellard, S. (2011). GATA6 haploinsufficiency causes pancreatic agenesis in humans. Nat. Genet. *44*, 20–22.

9. Stals, K.L., Wakeling, M., Baptista, J., Caswell, R., Parrish, A., Rankin, J., Tysoe, C., Jones, G., Gunning, A.C., Lango Allen, H., et al. (2018). Diagnosis of lethal or prenatal-onset autosomal recessive disorders by parental exome sequencing. Prenat. Diagn. *38*, 33–43.

10. Beriault, D.R., Dang, V.T., Zhong, L.H., Petlura, C.I., McAlpine, C.S., Shi, Y., and Werstuck, G.H. (2017). Glucosamine induces ER stress by disrupting lipid-linked oligosaccharide biosynthesis and N-linked protein glycosylation. Am. J. Physiol. Endocrinol. Metab. *312*, E48–E57.

11. Oslowski, C.M., and Urano, F. (2011). Measuring ER stress and the unfolded protein response using mammalian tissue culture system. Methods Enzymol. *490*, 71–92.

12. Livak, K.J., and Schmittgen, T.D. (2001). Analysis of relative gene expression data using real-time quantitative PCR and the 2(-Delta Delta C(T)) Method. Methods San Diego Calif *25*, 402–408.

13. Pfaffl, M.W. (2001). A new mathematical model for relative quantification in real-time RT-PCR. Nucleic Acids Res. *29*, e45.

14. Abu Bakar, N., Voermans, N.C., Marquardt, T., Thiel, C., Janssen, M.C.H., Hansikova, H., Crushell, E., Sykut-Cegielska, J., Bowling, F., MØrkrid, L., et al. (2018). Intact transferrin and total plasma glycoprofiling for diagnosis and therapy monitoring in phosphoglucomutase-I deficiency. Transl. Res. *199*, 62–76.

15. Ashikov, A., Abu Bakar, N., Wen, X.-Y., Niemeijer, M., Rodrigues Pinto Osorio, G., Brand-Arzamendi, K., Hasadsri, L., Hansikova, H., Raymond, K., Vicogne, D., et al. (2018). Integrating glycomics and genomics uncovers SLC10A7 as essential factor for bone mineralization by regulating post-Golgi protein transport and glycosylation. Hum. Mol. Genet. *27*, 3029–3045.

16. Kmiécik, D., Herman, V., Stroop, C.J., Michalski, J.C., Mir, A.M., Labiau, O., Verbert, A., and Cacan, R. (1995). Catabolism of glycan moieties of lipid intermediates leads to a single Man5GlcNAc oligosaccharide isomer: a study with permeabilized CHO cells. Glycobiology *5*, 483–494.

17. Chen, J., Li, X., Edmondson, A., Meyers, G.D., Izumi, K., Ackermann, A.M., Morava, E., Ficicioglu, C., Bennett, M.J., and He, M. (2019). Increased Clinical Sensitivity and Specificity of Plasma Protein N-Glycan Profiling for Diagnosing Congenital Disorders of Glycosylation by Use of Flow Injection-Electrospray Ionization-Quadrupole Time-of-Flight Mass Spectrometry. Clin. Chem. *65*, 653–663.